

# AllnGaAs Multiple Quantum Well-Integrated Device with Multifunction Light Emission/Detection and Electro-Optic Modulation in the Near-Infrared Range

Xin Li,\* Shuyu Ni, Yan Jiang, Jie Li, Wei Wang, Jialei Yuan, Dabing Li, Xiaojuan Sun, and Yongjin Wang\*

Cite This: *ACS Omega* 2021, 6, 8687–8692

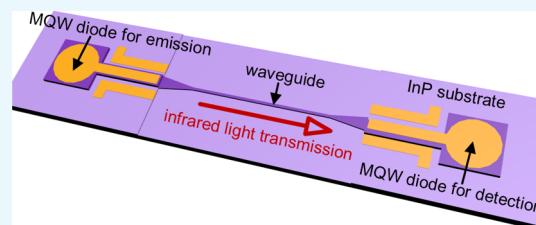
Read Online

ACCESS |

Metrics & More

Article Recommendations

**ABSTRACT:** A monolithic photonic chip with multifunctional light emission/detection and electro-optic modulation capabilities in the near-infrared range is proposed and realized on an InP-based wafer. Two identical AllnGaAs multiple quantum well (MQW) diodes operating independently as light emission/detection devices are fabricated using a two-step etching process on a single wafer and connected via a straight waveguide. The photocurrent induced in the MQW diode for the detection process is generated by the infrared light emitted by the MQW diode during the emission process and transmitted via the straight waveguide. The MQW diode has an electro-optic modulation characteristic, and its spectral responsivity exhibits a blueshift with an increasingly negative bias voltage under external infrared laser excitation. An on-chip communication test is conducted to study the potential applications of the proposed monolithic photonic chip for transmission of optical signals in the near-infrared range.



## INTRODUCTION

As the performance requirements for optoelectronic systems become increasingly high, the integration of multiple optical components to replace the conventional copper interconnects in single-function photonic chips is being researched in depth.<sup>1–3</sup> Monolithic photonic chips composed of different types of optical components integrated on a single wafer have multiple functions, including light emission, photodetection, optical transmission, and optical modulation.<sup>4–6</sup> The monolithic photonic chips intended for operation in the near-infrared range (1550 nm) have a wide range of potential applications in many fields, including optical communications, laser radar, and three-dimensional sensors.<sup>7–9</sup> Because commercial optical communication operates at 1550 and 1310 nm, compared with visible and ultraviolet light chips, infrared photonic chips are more easily compatible with commercial systems. However, infrared chips have their own limitations. Because the parameters such as carrier lifetime and carrier recombination efficiency of III-nitride materials for visible and ultraviolet light chips are better than that of InP and GaAs materials for infrared light chips, infrared chips cannot compete with visible and ultraviolet light chips in terms of communication transmission rate and modulation bandwidth.

Passive monolithic photonic chips for 1550 nm operation have been developed from single passive optical components into monolithic photonic chips with mature functions based on the silicon-on-insulator (SOI) material system over recent decades.<sup>10–13</sup> The first directional waveguide couplers on SOI

wafers with excess insertion losses of 1.9 dB for the 1550 nm wavelength were developed in the 1990s.<sup>14</sup> A fully integrated photonic network-on-chip circuit with wavelength-division multiplexing transceivers has recently been realized on an SOI wafer.<sup>15</sup> However, the indirect band gap of silicon means that the SOI wafer is unable to generate the required light emission and cannot be used to form the active optical components.<sup>16</sup> Therefore, the functionality of photonic chips on SOI wafers is generally incomplete. The light emission and detection functions for the entire photonic system must be realized using an off-chip equipment for photonic chips on SOI wafers. An external light source is usually coupled into the photonic chip via an optical fiber and the processed optical signal is then coupled from the photonic chip into photodetectors.<sup>17,18</sup> A monolithic photonic chip with complete functionality typically incorporates light sources and photodetectors based on III–V materials or germanium, and the SOI wafer is mostly used to form passive devices and modulators.<sup>19</sup> For example, Roelkens et al. demonstrated an InP/InGaAsP layer structure with III–V laser emission and photodetection

Received: February 5, 2021

Accepted: March 9, 2021

Published: March 17, 2021



for 1550 nm wavelength operation integrated on SOI waveguide circuits.<sup>20,21</sup> Inoue et al. reported the direct modulation characteristics of a membrane-distributed feedback laser for 1550 nm operation bonded on a Si substrate.<sup>22</sup> Although the research study noted above developed the active optical components on SOI wafers, complex bonding processes using polymers were inevitably introduced during the process of integrating the InP/InGaAsP epitaxial layer onto the SOI wafer. The possibility of fabricating a monolithic photonic chip operating in the near-infrared range based on InP-based materials with multiple quantum wells (MQWs) using a simple process is therefore attracting interest. Because MQWs offer both photoelectric and electro-optical conversion properties, InP-based materials with MQWs represent a promising choice for multifunction monolithic photonic chips in the near-infrared range.<sup>23,24</sup>

In this paper, we present a monolithic photonic chip on an InP-based wafer capable of multifunction light emission/detection and electro-optic modulation operations in the near-infrared range. Two identical AlInGaAs MQW diodes prepared on an InP-based wafer using a two-step etching process are connected via a straight waveguide, completely electrically isolated, and act independently as active optical devices. We investigate the photoelectric characteristics of the MQW diode for use in detection. The induced photocurrent is generated using the infrared light emitted by the MQW diode for emission and is then transmitted via the straight waveguide that connects the two MQW diodes. The MQW diode also has an electro-optic modulation characteristic. The spectral responsivity of the MQW diode for detection exhibits a blueshift with an increasing negative bias voltage when under excitation by an external infrared laser. Finally, we conduct an on-chip communication testing to study the potential application of the monolithic photonic chip for optical signal transmission in the near-infrared range.

The schematic shown in Figure 1a indicates the working mechanism of the AlInGaAs MQW-integrated device with its

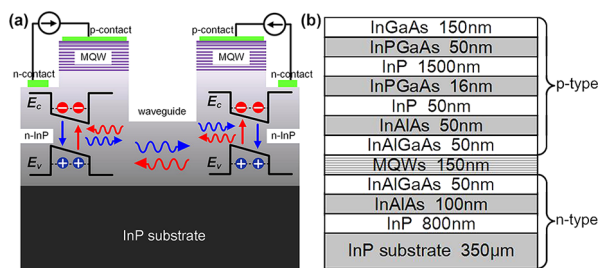


**Figure 1.** (a) Schematic of the AlInGaAs MQW-integrated device with multifunction near-infrared light emission and detection capability. (b) Cross-sectional schematic of the composition and thickness of the structure on the InP-based wafer.

multifunction near-infrared light emission and detection capability. The near-infrared light emission/detection functions are implemented on the two identical AlInGaAs MQW diodes. An MQW diode loaded using a positive bias operates in transmit mode and emits light in the infrared range. In contrast, the other MQW diode is loaded using a negative bias that causes it to operate in the receive mode and it absorbs the infrared photons transmitted via the waveguide connecting the two MQW diodes. Finally, the absorbed infrared photons generate electron–hole pairs in the MQWs, which lead to a

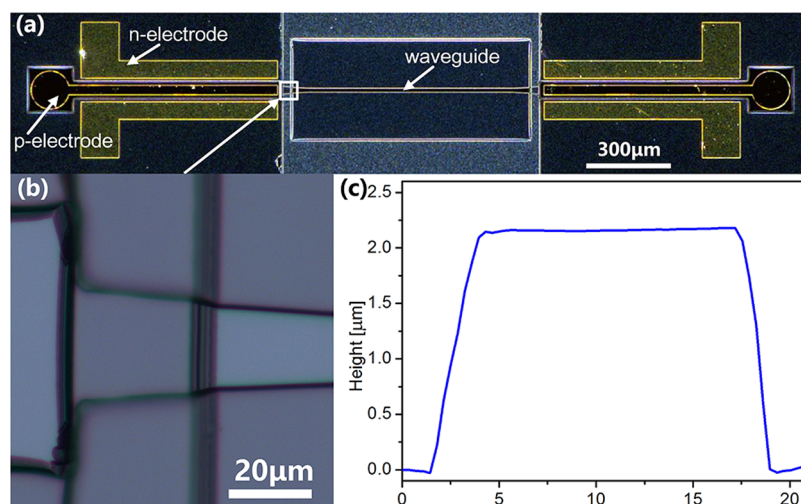
change in the internal electric voltage across the p–n junction. The AlInGaAs MQW-integrated device with the multifunction near-infrared light emission and detection capability is realized on a commercial InP-based wafer (Cengol Corporation, Beijing, China) using a double etching process. The composition and thickness of the structure on the InP-based wafer is shown in Figure 1b. The homogeneous epitaxial wafer substrate is composed of InP with a thickness of 350 μm. The epitaxial layers consist of ~800 nm thick InP, ~100 nm thick InAlAs, ~50 nm thick InAlGaAs, ~150 nm thick MQWs (five pairs of AlInGaAs MQWs), ~50 nm thick InAlGaAs, ~50 nm thick InAlAs, ~50 nm thick InP, ~16 nm thick InPGaAs, ~1500 nm thick InP, ~50 nm thick InPGaAs, and ~150 nm-thick InGaAs layers.

The fabrication process of the AlInGaAs MQW-integrated device is described as follows. The active areas of the two light emitting/detecting diodes and the straight waveguide connecting the two MQW diodes are patterned using photolithography and transferred to the InP-based wafer using inductively coupled plasma (ICP) etching for the III–V materials to expose the n-type layer. The gap for electrical isolation between the waveguide and the diodes is then patterned using photolithography and the p-type layer, and the MQWs of the gap area are removed by ICP etching of the III–V materials. The p and n electrodes with Ti (50 nm)/Pt (50 nm)/Au (400 nm) structures are formed using electron beam evaporation and lift-off processes.

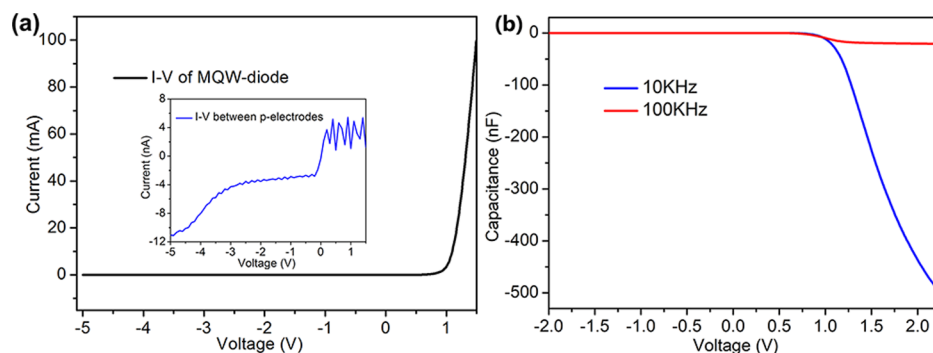
## RESULTS AND DISCUSSION

Figure 2a shows an optical microscopy image of the AlInGaAs MQW-integrated device with the multifunction near-infrared light emission and detection capability. The two identical AlInGaAs MQW diodes for the light emission/detection applications are connected using a straight waveguide to realize the transmission of the near-infrared light signals. The straight waveguide is 15 μm wide and 1000 μm long. Two tapered structures are located between the waveguides and the MQW diodes to couple light in and out of the MQW diodes. One end of each tapered structure has the same width (15 μm) as the straight waveguide and the other end of the tapered structure has a width of 30 μm. The gap between the MQW diodes and the straight waveguide for electrical isolation is shown in Figure 2b. According to the atomic force microscopy measurement data for the cross-sectional dimensions of the straight waveguide, as shown in Figure 2c, the width of the straight waveguide is 15 μm, as per the design value, and the height of the waveguide is 2.2 μm. The top and side walls of the straight waveguide are very smooth, and the sidewall angle is approximately 60°.

The electrical characteristics of the AlInGaAs MQW-integrated device were measured using a probe station connected to a semiconductor device parameter analyzer (Agilent, B1500A). Figure 3a shows the current–voltage (*I*–*V*) curves of the AlInGaAs MQW-integrated device. The turn-on voltage of a single MQW diode is approximately 0.87 V. The current of the MQW diode increases rapidly when the turn-on voltage is exceeded, and the current reaches 100 mA (the saturation value of the semiconductor device parameter analyzer) at a voltage of 1.5 V. The current between the p-electrodes of the two AlInGaAs MQW diodes varies from –12 to 8 nA, as shown in the inset of Figure 3a. The two MQW diodes are completely electrically isolated by the gap and can thus be regarded as independent devices. The capacitance–



**Figure 2.** (a) Optical microscopy image of AlInGaAs MQW integrated device; (b) magnified image of the gap between the MQW diode and the straight waveguide; (c) cross-sectional height profile of the straight waveguide.



**Figure 3.** Electrical performance of the AlInGaAs MQW-integrated device. (a) Measured  $I$ – $V$  curves of the AlInGaAs MQW-integrated device. (b) Measured  $C$ – $V$  curves of a single MQW diode.

voltage ( $C$ – $V$ ) curves of a single MQW diode shown in Figure 3b can be divided into two distinct regions. When the MQW diode is turned off in the negative voltage range, the capacitance remains at 0 nF. When the MQW diode is turned on at 0.87 V, the capacitance is a differential effect of the charge with respect to the forward voltage. As the forward voltage increases continuously, the radiative recombination exceeds the carrier diffusion, which leads to a negative variation of the injected carriers. The capacitance turns to a negative value according to the negative differential value of the charge. The capacitance is also modulated strongly by the frequency of the AC signal load on the MQW diode. As the AC signal frequency increases, the carriers from sub-band gap defects cannot follow the change of the AC signal. Then, the carriers will be trapped at the sub-band gap due to finite inertia. According to the Bansal–Datta-model, the carrier consumption at higher AC signal frequency reduces the absolute value of negative junction capacitance.<sup>25</sup>

The electroluminescence (EL) characteristics of the MQW diode were measured using a collimating mirror and a near-infrared spectrometer (Fuhan Optics, NIR 1700), with results, as shown in Figure 4a. A dominant EL peak is observed at 1512 nm. Because the current has a serious effect on the light output power of the MQW diode, the ratio between the peaks of the light output power at the currents of 10 and 2 mA is approximately 4.14. The MQW diode under a negative voltage bias operates as a photodetector in the near-infrared range, and

its spectral responsivity is measured by irradiating the MQW diode using a near-infrared laser source (Keysight, 81960A). As shown in Figure 4b, the MQW diode shows obvious electro-optic modulation characteristics. The spectral responsivity varies with the negative bias voltage applied to the MQW diode for detection. When the negative bias voltage increases from  $-4$  to 0 V, the dominant peak of the spectral responsivity shows a blueshift from 1541 to 1511 nm and the responsivity also presents an upward trend. The electro-optic modulation characteristics broaden the potential application range of the AlInGaAs MQW diode as a modulator in many fields including modulating retro-reflector communication, on-chip optical communications, and broad-spectrum infrared detectors.<sup>23,26</sup>

The normalized induced photocurrent of the MQW diode for detection shown in Figure 4c varies with the current applied to the MQW diode for an emission over the range from 2 to 10 mA. The MQW diode for emission converts the electronic signal into a modulated infrared light signal. The waveguide then transmits this light signal to the MQW diode for detection, which converts the received light signal into an electrical signal in the form of photocurrent. The power of the received light signal is modulated strongly by the current of the MQW diode for emission. When the current of the MQW diode for emission is under 10 mA, the photocurrent of the MQW diode for detection is approximately 613.2 nA, which is almost 5.2 times the value of the 117.9 nA photocurrent obtained at the 2 mA diode current. We also compared the EL

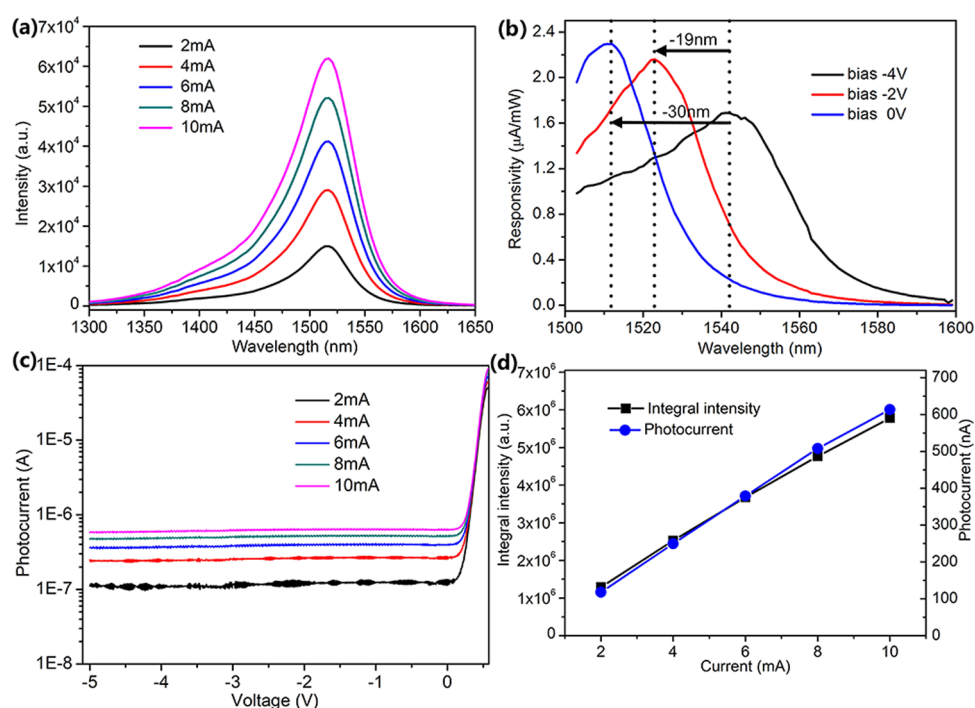


**Figure 4.** (a) EL characteristics of the MQW diode for emission vs current; (b) spectral responsivity of the MQW diode for detection as a function of the negative bias voltage; (c) induced photocurrent in the MQW diode for detection as a function of the current applied to the MQW diode for emission; and (d) EL integral intensity and induced photocurrent vs current characteristics.

integral intensity of the MQW diode for emission and the induced photocurrent of the MQW diode for detection versus the current of the MQW diode for emission to analyze the optical transmission stability of the straight waveguide, as shown in Figure 4d. When the current increases from 2 to 10 mA, the EL integral intensity and the induced photocurrent both increase linearly with the same slope. The straight waveguide can thus transmit near the infrared light with stable proportions between the two MQW diodes at different currents. The output light intensity can be modulated linearly using the value of the current. The integrated device thus presents a linear electro-optic modulation characteristic.

An on-chip communication test was also conducted to analyze the potential for application of the integrated device to optical communication. The transmit signal was loaded on the MQW diode for emission using an arbitrary waveform generator (Agilent, 33522A) with a 50 kbps random binary sequence. The offset voltage of the transmit signal was 1.2 V, and the voltage amplitude of the transmit signal was 20 mV. The light signal received was captured using the MQW diode for detection, which was connected via the straight waveguide, and the received light signal was then converted into an electrical signal. The transmitted signal and the received signal are shown in Figure 5a and demonstrate that the signal waveform is well preserved. The reverse voltage applied to the MQW diode for detection was 0 V. The open eye diagrams at 50 kbps for on-chip communication were clearly observed, as shown in Figure 5b. The capacitance of MQW diodes is a differential effect of charge with respect to forward voltage. The radiative recombination exceeds carrier diffusion as the forward voltage is increased, which leads to remarkable light emission as well as a negative variation of the injected carriers. The modulation bandwidth and transmission speed of the MQW diodes have a negative correlation with the RC time constant and the lower RC time constant is always

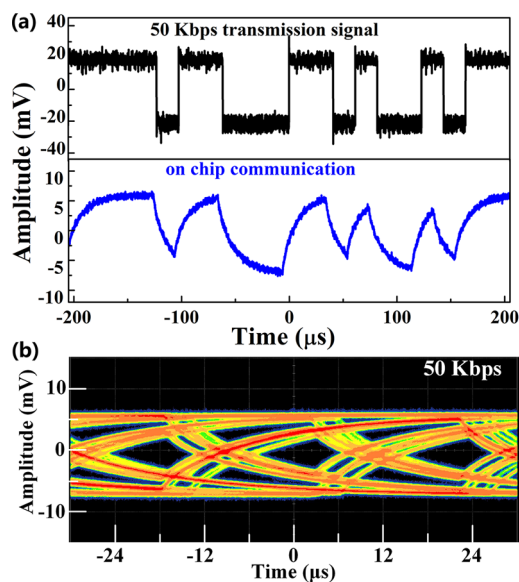


**Figure 5.** (a) Transmitted signal loaded on the MQW diode for emission with 50 kbps random binary sequence and received signal captured by the MQW diode for detection. (b) Eye diagrams measured at 50 kbps.

accompanied by the lower junction capacitance of MQW diodes. Hence, the absolute value of the negative junction capacitance of the MQW diodes is relatively high, as shown in Figure 3b, and could be the reason for the limited transmission speed of the integrated device in our study. As a result of the inevitable leakage current, the parasitic capacitance caused by the InP substrate under the MQW diodes may also increase the total capacitance. In future studies, we will focus on improving the transmission speed of the integrated device by

reducing the RC time constant of the MQW diodes by device structure optimization and other methods.

In conclusion, an AlInGaAs MQW-integrated device with multifunctional near-infrared light emission and detection has been realized on an InP-based wafer using a double etching process. One MQW diode is loaded using a positive bias voltage and operates in the transmit mode, emitting infrared light. The other MQW diode is loaded with a negative bias voltage, operates in the receive mode, and absorbs the infrared light transmitted via the straight waveguide that connects the two MQW diodes. A dominant EL characteristic peak of the MQW diode for emission is observed at 1512 nm. At a  $-3$  V bias voltage for the MQW diode for detection, the photocurrent realized at a current of 10 mA for the MQW diode for emission is approximately 613.2 nA, which is almost 5.2 times the 117.9 nA photocurrent obtained at a current of 2 mA for the MQW diode for emission. When the current increases from 2 to 10 mA, the EL integral intensity and the induced photocurrent both present linear increasing characteristics with the same slope. The straight waveguide realizes stable optical transmission between the two MQW diodes at different currents. In addition, the spectral responsivity varies with the negative bias voltage applied to the MQW diode for detection and the integrated device shows electro-optic modulation characteristics. When the negative bias voltage increases from  $-4$  to 0 V, the dominant peak of the spectral responsivity shows a blueshift from 1541 to 1511 nm and the responsivity also experiences an upward trend. An experimental on-chip communication test was also performed, and it provided a feasible approach to the development of integrated devices with multiple functionalities for a diverse range of applications.

## AUTHOR INFORMATION

### Corresponding Authors

**Xin Li** – Grünberg Research Centre, Nanjing University of Posts and Telecommunications, Nanjing 210003, China; [orcid.org/0000-0002-3370-013X](https://orcid.org/0000-0002-3370-013X); Email: [lixin1984@njupt.edu.cn](mailto:lixin1984@njupt.edu.cn)

**Yongjin Wang** – Grünberg Research Centre, Nanjing University of Posts and Telecommunications, Nanjing 210003, China; Email: [wangyj@njupt.edu.cn](mailto:wangyj@njupt.edu.cn)

### Authors

**Shuyu Ni** – Grünberg Research Centre, Nanjing University of Posts and Telecommunications, Nanjing 210003, China

**Yan Jiang** – Grünberg Research Centre, Nanjing University of Posts and Telecommunications, Nanjing 210003, China

**Jie Li** – Grünberg Research Centre, Nanjing University of Posts and Telecommunications, Nanjing 210003, China

**Wei Wang** – Grünberg Research Centre, Nanjing University of Posts and Telecommunications, Nanjing 210003, China

**Jialei Yuan** – Grünberg Research Centre, Nanjing University of Posts and Telecommunications, Nanjing 210003, China

**Dabing Li** – State Key Laboratory of Luminescence and Applications, Changchun Institute of Optics Fine Mechanics and Physics, Chinese Academy of Sciences, Changchun 130033, China; [orcid.org/0000-0001-5353-1460](https://orcid.org/0000-0001-5353-1460)

**Xiaojuan Sun** – State Key Laboratory of Luminescence and Applications, Changchun Institute of Optics Fine Mechanics and Physics, Chinese Academy of Sciences, Changchun 130033, China

Complete contact information is available at: <https://pubs.acs.org/10.1021/acsomega.1c00668>

## Notes

The authors declare no competing financial interest.

## ACKNOWLEDGMENTS

This work was jointly supported by National Natural Science Foundation of China (61531166004 and 11847022); China Postdoctoral Science Foundation (2018M640508); 1311 Talent Program of Nanjing University of Posts and Telecommunications; Natural Science Foundation of Jiangsu Province (BE2016186 and BK20170909). We thank David MacDonald, MSc, from Liwen Bianji, Edanz Editing China ([www.liwenbianji.cn/ac](http://www.liwenbianji.cn/ac)), for editing the English text of a draft of this manuscript.

## REFERENCES

- (1) Jalali, B.; Fathpour, S. Silicon Photonics. *J. Lightwave Technol.* **2006**, *24*, 4600–4615.
- (2) Rajan Philip, M.; Choudhary, D. D.; Djavid, M.; Bhuyian, M. N.; Bui, T. H. Q.; Misra, D.; Khreishah, A.; Piao, J.; Nguyen, H. D.; Le, K. Q.; Nguyen, H. P. T. Fabrication of Phosphor-Free III-Nitride Nanowire Light-Emitting Diodes on Metal Substrates for Flexible Photonics. *ACS Omega* **2017**, *2*, 5708–5714.
- (3) Koch, U.; Uhl, C.; Hettrich, H.; Fedoryshyn, Y.; Hoessbacher, C.; Heni, W.; Baeuerle, B.; Bitachon, B. I.; Josten, A.; Ayata, M.; Xu, H.; Elder, D. L.; Dalton, L. R.; Mentovich, E.; Bakopoulos, P.; Lischke, S.; Krüger, A.; Zimmermann, L.; Tsiokos, D.; Pleros, N.; Möller, M.; Leuthold, J. A Monolithic Bipolar CMOS Electronic–Plasmonic High-Speed Transmitter. *Nat. Electron.* **2020**, *3*, 338–345.
- (4) Gosciniak, J.; Atar, F. B.; Corbett, B.; Rasras, M. CMOS-Compatible Titanium Nitride for On-Chip Plasmonic Schottky Photodetectors. *ACS Omega* **2019**, *4*, 17223–17229.
- (5) Rickman, A. The Commercialization of Silicon Photonics. *Nat. Photonics* **2014**, *8*, 579–582.
- (6) Downs, C.; Vandervelde, T. Progress in Infrared Photodetectors Since 2000. *Sensors* **2013**, *13*, 5054–5098.
- (7) Knoll, D.; Lischke, S.; Zimmermann, L.; Heinemann, B.; Micusik, D.; Ostrovskyy, P.; Winzer, G.; Kroh, M.; Barth, R.; Grabolla, T.; Schulz, K.; Fraschke, M.; Lisker, M.; Drows, J.; Trusch, A.; Krüger, A.; Marschmeyer, S.; Richter, H. H.; Fursenko, O.; Yamamoto, Y.; Wohlfeil, B.; Petermann, K.; Beling, A.; Zhou, Q.; Tillack, B. Monolithically Integrated 25Gbit/Sec Receiver for 1.55 $\mu$ m in Photonic BiCMOS Technology. *Optical Fiber Communication Conference*; OSA: Washington, DC, 2014; p Th4C.4.
- (8) Mao, X.; Inoue, D.; Matsubara, H.; Kagami, M. Demonstration of In-Car Doppler Laser Radar at 1.55  $\mu$ m for Range and Speed Measurement. *IEEE Trans. Intell. Transp. Syst.* **2013**, *14*, 599–607.
- (9) Khan, I.; Rahman, M. Bending Loss Analysis of Optical Waveguide for SOI & SOS Material System towards Photonic Integration. *Proceedings of 4th Global Engineering Science & Technology Conference*, 2013; pp 1–8.
- (10) Li, P.; Sasaki, T.; Pan, L. F.; Hane, K. Comb-Drive Tracking and Focusing Lens Actuators Integrated on a Silicon-on-Insulator Wafer. *Opt. Express* **2012**, *20*, 627–634.
- (11) Li, A.; Wang, Z.; Liu, J.; Zeng, X. Low Cost Fabrication of SiO<sub>2</sub> Optical Waveguides by Laser Direct Writing on Ti-Doped Sol–Gel Films. *Opt. Lasers Eng.* **2011**, *49*, 351–355.
- (12) Trinh, P. D.; Yegnanarayanan, S.; Jalali, B. Integrated Optical Directional Couplers in Silicon-on-Insulator. *Electron. Lett.* **1995**, *31*, 2097–2098.
- (13) Zhuang, Y.; Chen, H.; Ji, K.; Hu, Y. On-Chip Hybrid Demultiplexer for Mode and Coarse Wavelength Division Multiplexing. *Appl. Phys. B* **2019**, *125*, 12.
- (14) Zhang, C.; Zhang, S.; Peters, J. D.; Bowers, J. E. 8  $\times$  8  $\times$  40 Gbps Fully Integrated Silicon Photonic Network on Chip. *Optica* **2016**, *3*, 785.
- (15) Reed, G. T.; Knights, A. P. *Silicon Photonics*; John Wiley & Sons, Ltd.: Chichester, UK, 2008.

(16) Zou, Y.; Subbaraman, H.; Chakravarty, S.; Xu, X.; Hosseini, A.; Lai, W.-C.; Wray, P.; Chen, R. T. Grating-Coupled Silicon-on-Sapphire Integrated Slot Waveguides Operating at Mid-Infrared Wavelengths. *Opt. Lett.* **2014**, *39*, 3070.

(17) Roland, I.; Zeng, Y.; Checoury, X.; El Kurdi, M.; Sauvage, S.; Brimont, C.; Guillet, T.; Gayral, B.; Gromovyi, M.; Duboz, J. Y.; Semond, F.; de Micheli, M. P.; Boucaud, P. Near-Infrared III-Nitride-on-Silicon Nanophotonic Platform with Microdisk Resonators. *Opt. Express* **2016**, *24*, 9602.

(18) Fathpour, S. Emerging Heterogeneous Integrated Photonic Platforms on Silicon. *Nanophotonics* **2015**, *4*, 143–164.

(19) Koester, S. J.; Schaub, J. D.; Dehlinger, G.; Chu, J. O. Germanium-on-SOI Infrared Detectors for Integrated Photonic Applications. *IEEE J. Sel. Top. Quantum Electron.* **2006**, *12*, 1489–1502.

(20) Roelkens, G.; Van Thourhout, D.; Baets, R.; Nötzel, R.; Smit, M. Laser Emission and Photodetection in an InP/InGaAsP Layer Integrated on and Coupled to a Silicon-on-Insulator Waveguide Circuit. *Opt. Express* **2006**, *14*, 8154.

(21) Roelkens, G.; Zhang, J.; Muliuk, G.; Goyvaerts, J.; Haq, B.; de Beeck, C. O.; Liles, A.; Wang, Z.; Dhoore, S.; Kumari, S.; Juvert, J.; Van Campenhout, J.; Kuyken, B.; Van Thourhout, D.; Corbett, B.; Trindade, A. J.; Bower, C.; Baets, R. III-V/Si PICs Based on Micro-Transfer-Printing. *Optical Fiber Communication Conference (OFC) 2019*; OSA: Washington, DC, 2019; p W4E.6.

(22) Inoue, D.; Hiratani, T.; Fukuda, K.; Tomiyasu, T.; Amemiya, T.; Nishiyama, N.; Arai, S. High-Modulation Efficiency Operation of GaInAsP/InP Membrane Distributed Feedback Laser on Si Substrate. *Opt. Express* **2015**, *23*, 29024.

(23) Arslan, Y.; Colakoglu, T.; Besikci, C. Diffraction-Grating-Coupled High Quantum Efficiency InP/InGaAs Quantum Well Infrared Photodetector Focal Plane Array. *IEEE J. Quantum Electron.* **2013**, *49*, 186–195.

(24) Ferreira, R. X. G.; Xie, E.; McKendry, J. J. D.; Rajbhandari, S.; Chun, H.; Faulkner, G.; Watson, S.; Kelly, A. E.; Gu, E.; Penty, R. V.; White, I. H.; O'Brien, D. C.; Dawson, M. D. High Bandwidth GaN-Based Micro-LEDs for Multi-Gb/s Visible Light Communications. *IEEE Photonics Technol. Lett.* **2016**, *28*, 2023–2026.

(25) Bansal, K.; Datta, S. Voltage modulated electro-luminescence spectroscopy to understand negative capacitance and the role of sub-bandgap states in light emitting devices. *J. Appl. Phys.* **2011**, *110*, 114509.

(26) Goetz, P. G.; Rabinovich, W. S.; Mahon, R.; Murphy, J. L.; Ferraro, M. S.; Suite, M. R.; Smith, W. R.; Xu, B. B.; Burris, H. R.; Moore, C. I.; Schultz, W. W.; Mathieu, B. M.; Hacker, K.; Reese, S.; Freeman, W. T.; Frawley, S.; Colbert, M. Modulating Retro-Reflector Lasercom Systems at the Naval Research Laboratory. *Proceedings—IEEE Military Communications Conference MILCOM*, 2010; pp 1601–1606.